Cell stiffness assessment based on nuclei morphological response to patterned surfaces

Inês Santos

Tissue Regeneration Group, MIRA Institute, University of Twente, Netherlands

Abstract Diseased cells, as cancerous cells, tend to present an abnormal morphology. Several studies had already used cell stiffness as a cell marker and a diagnostic parameter for cancer. It is known that stiffness from cancerous cells is related to metastatic potential. To diagnosis metastatic cancer on early stages, material surface topography was used, since it is able to evoke specific cellular responses.In this study, we assessed cellular stiffness based on nuclei response to patterns. We modulated this property, treating hMSCs with Blebbistatin and Trichostatin A, on flat and two patterned surfaces. Thus, based on principal component analysis, surface Pat.S.1 was determined to be better than Pat.S.2. We further used Pat.S.1 to distinguish different cell types, according their responses to the surface. Lamin-A:Lamin-B ratio of different cell types, was calculated to assess nuclear stiffness. This allowed us to conclude that nuclei deformed according to their stiffness. Results proved the possibility to evaluate cell stiffness according to nuclei morphological responses to patterns. Although, further study should be done to find the most optimal morphological descriptors, for different types of cells.

Keywords: Cancer, hMSCs, Blebbistatin, Trichostatin A, Patterned surfaces, Cell stiffness, Nuclei response, Nuclear lamins.

1 Introduction

1.1 Influence of cell shape on cell function

Mesenchymal stem cells (MSCs) are capable to differentiate into many cell types, such as osteoblasts (bone cells), chondrocytes (cartilage cells) and adipocytes (fat cells), meaning that these multipotent cells are the precursor of cells for different connective tissue cells. Although, the phenotype of cells from different tissues differ greatly. These different cell morphologies are thought to arise from a combination of biological, physical and chemical cues in the stem cell microenvironment, during stem cell commitment, the process by which a cell chooses its fate [1], [2].

The physical properties of cells is challenging, and while genetic and biochemical aspects of development were intensely studied in the past, the contribution of physical properties is poorly understood in many processes. Physical cues have been recognized as crucial factors in regulating cell fate [1]. Cell shape is determined by the mechanical balance of the forces exerted on the cell membrane by intracellular components and the outside environment, such as the adhesion to neighboring cells, to the extracellular matrix (ECM) and its properties. Essentially, all of these factors are integrated via biochemical signaling pathways and result in distinct physical properties of cells and tissues [3].

The mechanotransduction is the molecular mechanism by which cells respond to changes in their physical environment by 'translating' mechanical stimuli into biochemical signals [4]. So, cells can sense mechanical stimulation and changes in their physical environment through force-induced conformational changes on the molecular level, called mechanosensing [5]. The downstream pathways of mechanotransduction can result in the opening of stretch sensitive ion channels, reorganization of the cytoskeleton which can result on force generation by the cell, mechanoresponse [6]. Figure 1 illustrates these events described above.

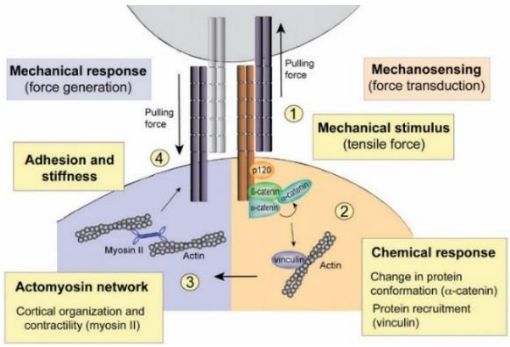

Figure 1 - Mechanosensing, mechanotransduction and mechanoresponse representation.

1.2 Cytoskeleton mechanics

The internal cytoskeletal architecture alters deeply cell shape. The cytoskeleton of cells is a three-dimensional interconnected filaments network that is responsible for maintaining cell shape and to provide mechanical rigidity.

On a flat surface, the cells basically flattens, which result from a spherical shape in suspension to a spread shape when attached to the surface [8]. On a microstructure surface, the cells look for the maximum of contact to the surface, result from the stretching of the cytoskeleton filaments above the nucleus. For these changes in shape were proposed two possible mechanisms. One would end in a pushing down of the nucleus on the surface. The other would result in a pulling down of the nucleus by the connection of cell attachment sites formed to the edges and sides of the microstructures, to the nucleus through the cytoskeleton [9]. In Figure 2 is schematically indicated these two proposed mechanisms.

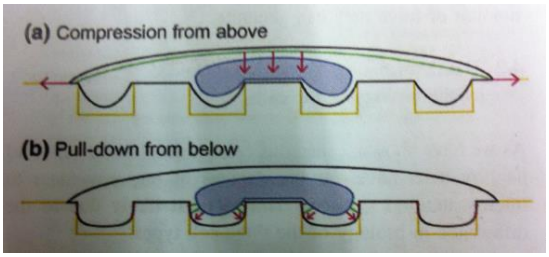

Figure 2 - Representation of nucleus deformation by the cytoskeleton in microstructure surfaces [9].

Myosin II is an actin-binding protein that has actin cross-linking and contractile properties [10]. This protein is an ATP-dependent motor protein, also known as conventional myosin, responsible for tension generation and maintenance of pre-stress in the cytoskeleton [11]. Several studies were performed to understand the way myosin II activity controls nuclear shape and stiffness. As example, in the presence of Blebbistatin, an inhibitor of actomyosin contractility, cells tend to adopt a more rounded nucleus [12] and to decrease their stiffness.

It was reported that the regulation of nucleus shape is made through a subset of highly organized and oriented actomyosin fibers that covers the top of the nucleus, forming the perinuclear actin cap. This structure is physically connected to the nuclear envelope through LINC complexes, and could be disorganized or eliminated by actmyosin contractility inhibitors, LINC complexes rupture or depletion of nuclear lamin A/C [13].

2 Nuclear mechanics

One of the most fundamental problems in tissue morphogenesis is the question of how changes in cell shape produce alterations of nuclear form and functions.

The nucleus is generally the largest organelle and it is 2 to 10 times stiffer than the cytoplasm [15], and it is affected by intra- and extracellular forces transmitted through the cytoskeleton. The nucleoplasmic surface of the inner nuclear membrane is lined with the nuclear lamina, a fibrous network of proteins. These intermediate lamin filaments help to connect lamins to chromatin structures, the nuclear interior [16].

Lamins are the main component of the nuclear lamina. This thin layer of intermediate filaments provides mechanical support to the nucleus, contributing to nuclear stiffness and nuclear stability [17]. Beyond that, lamins regulate and support protein complexes involved in DNA replication, cell division or chromatin reorganization [15]. Lamins are divided into A-type lamins (lamins A and C) and B-type lamins [6].

As previously shown, knocking down lamin A/C on nuclei can lead to nuclear stiffness decrease and consequently to cell stiffness [18].

Unlike lamin A/C, lamin B dominates in soft tissue. The stoichiometric ratio of lamins A and B is a fair indicator of how these intermediate filament proteins contribute to nuclear stiffness. As reported in literature [17], several cell types were scaled according to their nuclear stiffness, lamin-A:lamin-B stoichiometric ratio and tissue microelasticity (measured in kPa), as shown by Figure 3. The use of lamin-A:lamin-B ratio is a good method to model differ cell types according their nuclear stiffness.

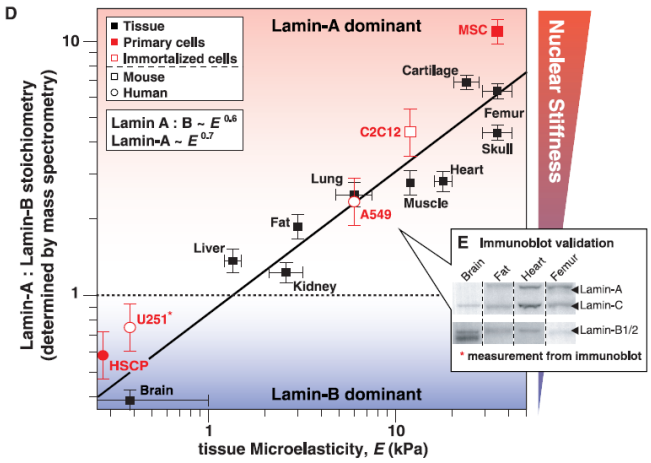

Figure 3 - Schematic representation of correlation between lamin-A:lamin-B ratio, nuclear stiffness and tissue microelasticity for different tissues and cell types [17].

2.1.1 Nucleus interior

The interior of the nucleus is mainly composed of chromatin that occupies a considerable amount of its volume [6]. The nucleosomal structure involves a very long double-stranded deoxyribonucleic acid (DNA) wrapped around small basic proteins termed histones. Functional alterations of the histone tails affect the response of chromatin, regarding her compaction state [19]. Changes in histone modifications have also been linked to nuclear size and shape. The interaction histone-DNA is regulated by a class of enzymes designed histone deacetylases (HDACs). Trichostatin A (TSA) is a common HDAC inhibitor, which enhances the acetylation of histones, weakening the histone-DNA interaction. Thus, chromatin becomes less compacted and as consequence, DNA becomes more available for the transcription process [20].

2.2 Cell morphology as marker during disease

It is known from different studies that cells during diseases could present abnormal morphology comparing with normal cells. Through these morphological differences, diseased cells have been identified [21].

The cytoskeleton is characteristically altered in many diseases, including cancer. Once mechanical properties of human cells, as mechanical strength and morphology, are largely governed by the cytoskeleton, cellular stiffness has been used as a cell marker and a diagnostic parameter for disease. [21].

Furthermore, abnormal nuclear shapes are also associated with cancer [23]. Routine detection techniques based on light microscopy have been developed in order to detect cancer in its early stages of development. Although it remains difficult to explain the exact relationship between nuclear morphology and cancer. A hypothesis based on mechanical arguments have been suggested. The mechanical approach suggest that severe modifications of the shape and mechanical properties of the nucleus can facilitate the ability of cells to transit through narrow constrictions that are smaller than the nuclear diameter and thus promote the formation of metastases. For this reason, it is well known that cancer cell lines, such as SaOs-2, have been shown to be more deformable than healthy cells [8].

Several studies found that cancer cells with higher migratory and invasive potential are less stiff than cells with a lower migration and invasion potential.

The studies of mechanical properties of cancer cells can lead to discovering new targets for cancer.

2.3 Techniques to study cell and nuclear mechanics

As described above, mechanical properties of cells plays a crucial role for many cell functions and can vary from cell type to cell type, or in the course of differentiation, or due to disease. A number of different tools have been developed in the last decades that allow the measurement of rheological properties of living cells [24]. Rheology is the technique that measures how materials deform or flow in response to applied mechanical forces [25].

To measure global rheological properties of cells like their overall, several techniques have been established, such as, micropipette aspiration, microplate manipulation, optical stretching, microfluidic deformation, microrheology and atomic force microscopy (AFM), magnetic twisting cytometry.

2.4 Topographic surfaces as an alternative tool

It was shown that cells have a diverse respond to different topographies. At the same time, the respond of different cell types to same patterns is varied. These different responses can be detected by cell morphology assessment [26], [27].

The knowledge about interactions cell-material still needs to be developed, since identifying a surface topography that induce desired cell behavior ("hit" surfaces [28]) is a very hard task. Therefore in the past ten years, emerged a new set of tools, combinatorial and high-throughput screening, in polymeric biomaterials development [29].

A platform for high-throughput screening of material surface topographies was developed. It consists in a library of 2176 distinct surfaces, randomly selected by mathematical algorithms (Figure 4-A). These topographical designs were reproduced in duplicate on 2x2 cm^2 chip, called TopoChip (Figure 4- C), in rectangular areas of 290x290 μm^2, called TopoUnits (Figure 4-B), of any desired material. Each topographical surface was algorithmically constructed by a specific feature. A feature is made up of a variable number of three primitive shapes: circles, triangles and rectangles (Figure 4-B). Cells are seeded on the chip and cultured for the intended period of time, and then TopoChip is imaged via fluorescence microscopy. Image analysis is performed using Cell Profiler (CP), in order to describe the response of the cells, using various descriptors describing both the cell and nucleus shape, to each of the surface on the chip, at a single-cell level [28].

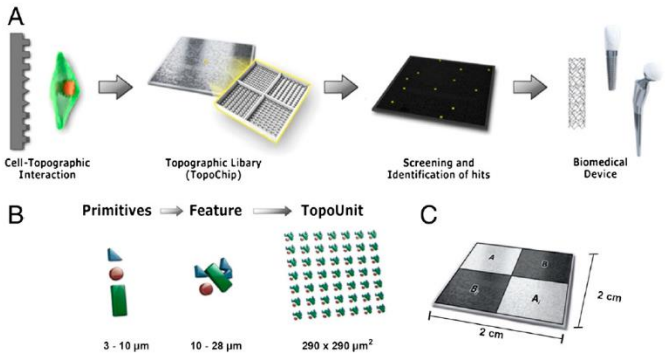

Figure 4 - TopoChip design. (A) Schematic representation of a sequence events from initial design of TopoChip to clinical application. (B) TopoUnit constitution. (C) TopoChip division. [28].

TopoChip is a very versatile approach, which allows to assess cell response to more than 2000 random generated patterns.

3 Materials and Methods

3.1 Substrate Fabrication

The patterned surfaces that were used were fabricated by a spin-off company from UT called Materiomics. The fabrication process for the patterned discs used is the same as for TopoChips, which was deeply approached in the section 2.4. The patterned surfaces used were one of the surfaces from TopoChip design, and it was enlarged to discs. Thus the discs presented one of the 2176 distinct surfaces topographies of the TopoChip [28] and were made of polystyrene.

3.2 Patterned surfaces selection

To select the patterned surface to use in the project, it was important that nuclei morphology of hMSCs was less affected as possible by surface, so that the morphological changes of the nuclei were due to changes in their stiffness, caused by drugs treatments.

After image analysis of patterns on TopoChip, it was selected the ones that have patterns close to each other, and then it was observed nuclei morphology of hMSCs in that patterns, from previous screens, and it was selected two surfaces that have slightly unchanged nuclei.

3.3 Cell Culture

HMSCs, donor 117 and donor 130 of TR donor bank (D117 and D130, respectively) were cultured in MEM Alpha medium (*Life Technologies, Gibco*) supplemented with 10% FBS (Lonza), 2mM L-glutamine (*Life Technologies, Gibco*), 100 U/ml Penicillin-Streptomycin (*Life Technologies*) and 0,2 mM ascorbic acid (*Sigma Aldrich*). SaOs-2 cells, hDFs and hCHs were cultured in DMEM medium (*Life Technologies, Gibco*). For SaOs-2 cells and hDFs the medium was supplemented with 10% FBS (Lonza) and 100 U/ml Penicillin-Streptomycin (*Life Technologies*), for hCHs the medium was supplemented with 10 % FBS (Lonza), 1% *MEM NEAA* (*Life Technologies, Gibco*), 1% ascorbic acid (*Sigma Aldrich*), 100 U/ml Penicillin-Streptomycin (*Life Technologies*) and 1% proline. HUVECs were cultured in EBM-2 medium *(Lonza, Clonetics*) and MDA-MB231 cells were cultured in DMEM/F-12 (*Life Technologies, Gibco)*

supplemented with 5% FBS e 100 U/ml Penicillin-Streptomycin (*Life Technologies*).
Routinely, the culture media were exchanged every two days.

3.4 Drug Treatments

To test different forces that have an influence on nuclei morphology, cells were treated with different drugs, Blebb and TSA. The two inhibitors were diluted in DMSO and were also further diluted in complete medium. So the control for these drug treatments was cells treated with DMSO.
HMSCs were seeded for 48h, and during the last 24h with DMSO (Bebb+TSA volumes) Blebb (50 µM), TSA (0,2 µg/ml) and Blebb+TSA (50 µM + 0,2 µg/ml).

4 Cell staining

4.1.1 Actin and DNA staining

Cells were washed once with prewarmed PBS and fixed in prewarmed 4% (v/v) paraformaldehyde in PBS for 10 min at RT. The fixative was removed and cells were washed two times with PBS. To permeabilize the cells were incubated for 10 min in 0,1% (v/v) triton X-100 (*Sigma-Aldrich*) in PBS and washed twice afterwards. For blocking, cells were treated with a 5% (m/v) solution of BSA for 30 min at RT, to avoid unspecific labeling and after they were washed twice with PBS. Phalloidin-AF594 (*Invitrogen*) was diluted in a relation 1:200 in PBS and 150 µl were pipetted on a petri dish. Each glass slide or patterned surface were placed face down in each drop of 150 µl and the cells were incubated for 1h at RT in the dark. Then, the glass slide or patterned surface was removed and placed again in the well and the cells were washed three times in PBS. A small amount of a solution with 1:100 of DAPI in PBS were placed in each well and cells were covered for 10 min at RT in the dark. Cells were washed twice with PBS and subsequently the scaffolds were mounted in microscopic slides with on drop of Mowiol mounting medium (*Sigma-Aldrich*). The slides were kept on RT in the dark for 2h to allow the mounting medium to dry and the imaged immediately or stores at 4 ºC.

4.1.2 Lamin A/C and Lamin B staining

The first steps of this staining were similar with the first steps of the actin and DNA staining, but the protocol was adjusted and adopted from the literature [17]. Time of fixation was increased to 20 min, the permeabilization was with 0,5% (v/v) triton X-100 for 20 min and the blocking was during 1 h. After the blocking step, cells were incubated with primary antibodies, Lamin A/C (636, *Santa Cruz Biotechnology* sc-7292) and Lamin B (M-20, *Santa Cruz Biotechnology* sc-6217), at a dilution of 1:300 in 2% (v/v) BSA in PBS overnight at 4 ºC. Then, secondary antibodies, goat anti-mouse Alexa-Fluor 594 (*Invitrogen*) and donkey anti-goat Alexa-Fluor 488 (*Invitrogen*), were diluted at 1:500 in PBS, and a drop was covered the cells for 1,5 h at RT in the dark. Cells were after washed three times with PBS and the samples mounting were performed equal as the mounting step of actin and DNA staining described in section 4.1.1.

4.2 Fluorescence Imaging and Analysis

Fluorescence images were obtained using a BD Pathway 435 microscope or a Nanozoomer 2.0-RS (Hamamatsu).
For capturing cell morphology, it was used open sourced software Cell Profiler (CP) [30]. DAPI channel was used for identification of individual cell nuclei, while cells cytoplasm were identified by Phalloidin channel. After identification of individual cells, their morphological measurements were performed.
The Cell Profiler data were imported into Prism 5.01 software (GraphPad) or into R software and then plotted. Some data from CP were analyzed by recursive partitioning analysis and principal component analysis.
Some samples treated with TSA were imaged by a Nikon A1 confocal microscope. Vertical confocal image stacks were recorded to visualize cell morphology on patterns, and the images were recorded with 100x oil objective. Using the Image J 1.48v software, 3D-images were built.

4.3 Statistical analysis

The statistical analysis were performed by one-way ANOVA using Kruskal Wallis test, and statistical significance was considered at p-value<0,05.

5 Results and Discussion

5.1 Optimization of hMSCs densities

To study different responses of hMSCs to different conditions, fluorescence images were analyzed by Cell Profiler software, that gives descriptors of cell and nucleus shape that characterize cell response at a single-cell level. Hence it is important to decide the most appropriate cell density for cell seeding.
For this, hMSCs were seeded on glass slides, in three different densities, and were immunostained in order to observe single cells and to investigate the influence of cell density.

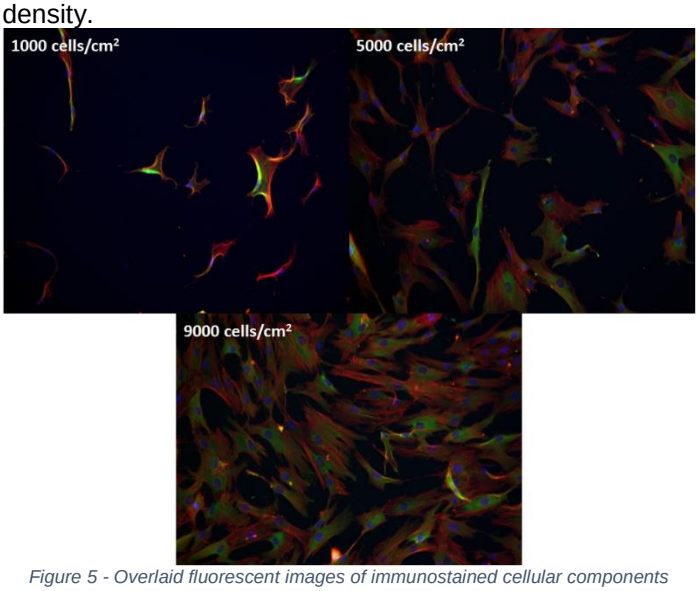

Figure 5 - Overlaid fluorescent images of immunostained cellular components (merged) for different cell densities. AlexaFluor 594 labeled F-actin (red), AlexaFluor 488 labeled vinculin (green), and DAPI nuclear staining (blue).

By the observation of Figure 5, it was possible to note that with the highest cell density (9000 cells/cm^2), the individualization of each cell became difficult by eyes, thus for the software (Cell Profiler) was also a complicated task.

So there is a higher probability of individual cells identification be poorly made. For the other two cell densities (1000 and 5000 cells/cm^2), the identification of single cells was easier, since they were not so close to each other compared to the highest density (Figure 5). However, it was decided to use the cell density of 5000 cells/cm^2 for hMSCs in further studies, by the reason that with this cell density was possible to identify easily single cells and principally because there were more cells per image to analyze, conferring more solidity to the studies. This cell density was commonly used in works that use micropatterning techniques to study some behaviors of hMSCs [1], [31], as had been done in later studies of this work.

5.2 Optimization of Blebb treatment

To modify hMSCs stiffness, it was used an inhibitor of myosin II, as mentioned in section 1.2. First Blebb was added in three different concentrations and in two different time point, in order to evaluate its effect on hMSCs, but the principal goal of this experiment was to find the optimal concentration and time point for further experiments.

HMSCs were treated with Blebb at 12,5 µM, 25 µM and 50 µM for 24h or 2h, as stated at the literature [32]. The following pictures show the effect of Blebb on hMSCs at different conditions.

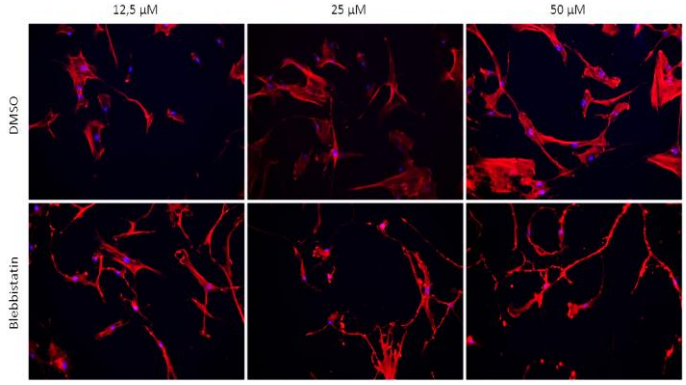

Figure 6 - Blebb effect on hMSCs for 24h, at three different concentrations (12,5 µM, 25µM and 50 µM).

According to Figure 6, comparing the control situation (DMSO) with Blebb treatment, it was observed that cells treated for 24h, lost cytoplasmic coherence and also presented a more dendritic shape. These shape changes are due to the Blebb effect on actomyosin contractility of cells, which means that cells lose their cytoplasmic contractility [32]. A comparison between the three different concentrations of this inhibitor showed that the highest concentration had an effect more relevant on cells cytoplasm than the other lowest concentrations.

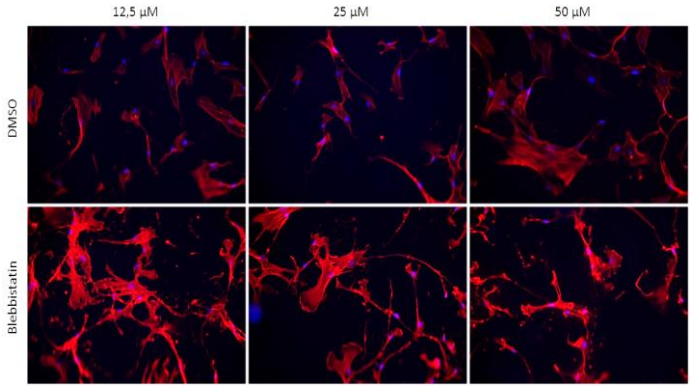

Figure 7 - Blebb effect on hMSCs for 2h, at three different concentrations (12,5 µM, 25µM and 50 µM).

For the other time point, as shown in Figure 7, the cells treated also presented a lack of lost cytoplasmic coherence compared with cell in control situation. However, the differences between the three different concentrations of Blebb were not so evident, in contrast with the first time point, as mentioned above.

For all these reasons, it was decided that the optimal time point was the first one, Blebb treatment during 24h, and the optimal concentration of the inhibitor was 50 µM, since cells in these conditions presented a dendritic shape more pronounced. This means that cell stiffness decreased and so it was possible to modulate this cellular property.

5.2.1 Cell and nuclei morphological descriptors

In this project, the assessment of cell stiffness could be done based on cell morphology (F-actin) or on nuclei morphology. The next figure shows two graphs of one Cell Profiler area shape parameter (Solidity), for cell and nuclei, in different conditions of Blebb treatment. Solidity was chosen because by its graphs, in Figure 8, it was possible to see the variations of each condition on cell, and on nuclei these variations are not so evident.

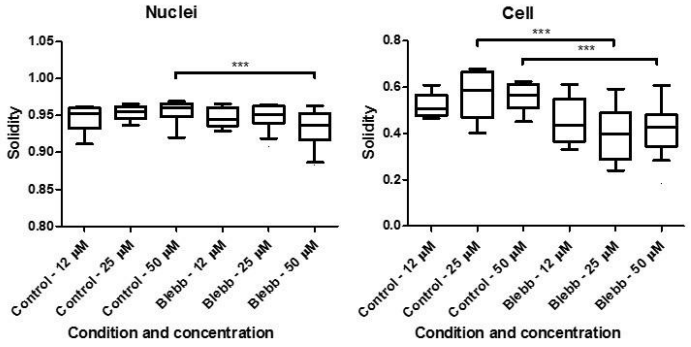

Figure 8 - Representation of the parameter Solidity for cell and nuclei shape, of the first time point of Blebb treatment. Statistical analysis by One-way ANOVA (Kruskal Wallis test) showed significance at p-value<0,05.

From Figure 8, it was clear to see differences between conditions, both in cell and nuclei morphology. Hence, differences in cell morphology were stronger and could capture differences in low dosage of Blebb. It was decided to stick to measurements in nuclei morphology, as DAPI staining, since for future diagnostics this technique will be cheaper. Further, the measurements for control conditions for nuclei were more consistent than for cells.

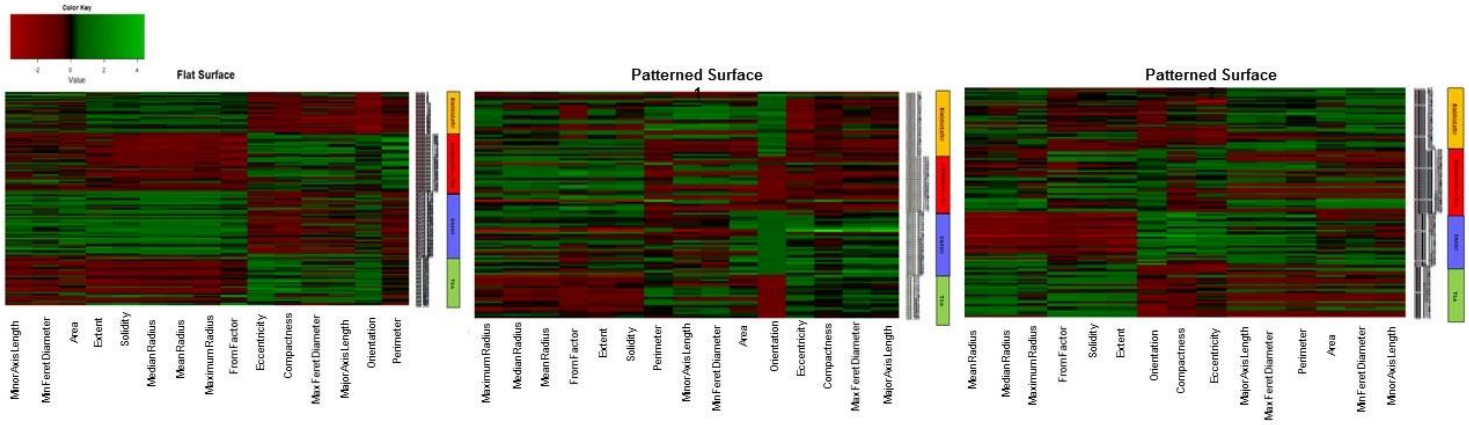

Figure 9 - Heat maps for all nuclei morphological descriptors, in columns, for each treatment, in rows, in each surface. Each parameter were scaled in a range from -5 to 5, where 0 is median of nuclei response.

5.3 Drug treatments and Patterned surface validation

This experiment had two main goals. One was to evaluate the joint effect of Blebb and TSA on cell response and on nuclei morphology. The other goal was to validate which patterned surface was better for further project experiments. For that, cell seeding was done on a flat surface (control situation) and on two selected patterned surfaces. The patterned surfaces selection was explained in section 3.2.

5.3.1 Blebb and TSA treatments

As said in section 1.2., perinuclear actin cap has an important role in the regulation of nucleus shape and its positioning, so hMSC's were treated with Blebb and TSA together, to test if actin cap was destroyed. It was assumed that, since TSA is an inhibitor of histone deacetylase causing DNA decondensation, cells treated with TSA will present nuclei bigger compared with control, as shown in literature [20]. Cells treated with Blebb and TSA will probably have the biggest nuclei, once Blebb decreases contractility of actin filaments and TSA increases nucleus volume. Figure 10 represents schematically these assumptions.

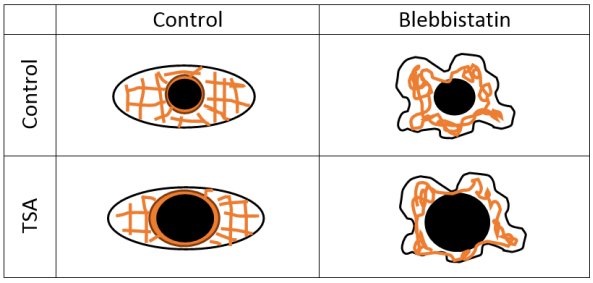

Figure 10 - Schematic representation of Blebb and TSA hMSCs treatment on flat surface.

The Figure 9 shows heat maps, in order to better visualize the responses of nuclei to each surface.

After performing the Cell Profiler analysis of the images of this experiment, it was made a recursive partitioning analysis to select the most descriptive parameters of each condition (DMSO, Blebb, TSA and Blebb+TSA in the three surfaces). According to cell (F-actin) and nuclei morphology, several parameters were selected. For the nuclei were, FormFactor, MedianRadius, Solidity, Extent, MinFeretDiameter, MaxFeretDiameter, MeanRadius and Eccentricity. For the cell were, FormFactor, MedianRadius, Solidity, Extent, Perimeter, MajorAxisLength, Compactness, MinorAxisLength and MinFeretDiameter. In discussion we give more emphasis on nuclei responses since it was decided to use nuclei morphology descriptors to assess cell stiffness.

By observation of Figure 9, it was seen clearly that on different surfaces, cells respond differently at same condition, as descriptors of morphology showed (columns). These different responses to different surfaces are good evidences for further studies to assess cell stiffness based on nuclei morphology. In fact, these responses differ mainly, when patterned surfaces were compared to flat surface.

In order to show the results of Cell Profiler analysis of this experiment, it was selected two parameters that describe in general nuclei responses to the different conditions, on flat surfaces. It was shown the responses on flat surface, since in these surfaces was possible to evaluate only the effect of the different conditions on responses, and not also the effect of the surface, as in case of patterned surfaces. The graphs of the parameters are represented in Figure 11.

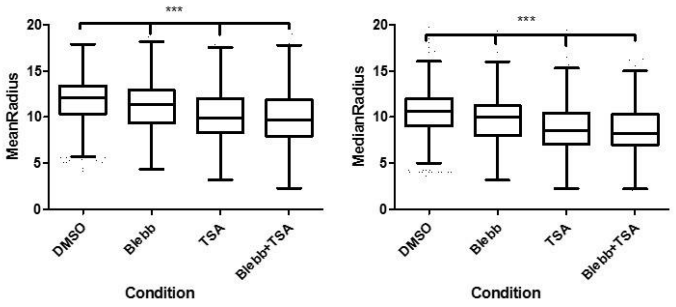

Figure 11 - Representation of MeanRadius and MedianRadius for nuclei in the different conditions (DMSO, Blebb, TSA and Blebb+TSA) on flat surface. Statistical analysis by One-way ANOVA (Kruskal Wallis test) showed significance at p-value<0,05.

Area would probably be a good parameter to describe the influence of each inhibitor in this experiment, as Figure 10 represents. Although Area was not selected by the recursive partitioning analysis. So MeanRadius and MedianRadius were the parameters chosen to explain cell

and nuclei responses to each condition, because they were probably good parameters to correlate with Area. Through Figure 11 was possible to see that the parameters values decrease with treatments (Blebb, TSA and Blebb+TSA) compared with values of the control condition (DMSO). In the control situation the nucleus was undergo actin force, consequently actin compressed the nucleus from above through the spreading forces exerted on the cell. Projected nucleus area will be bigger comparing with Blebb treatment, where actin didn't provide force and the nucleus became less spread. With TSA, the radius values were even less, which could be explained by the force that DNA decondensation did, be higher than the force exerted by actin. For this reason, the nucleus was less spread, being the Area seen from top lower, and consequently MeanRadius and MediusRadius values too. About Blebb+TSA condition was difficult to take conclusions, being the responses an intermediate behavior of Blebb and TSA conditions.

Thus, according to these reasons, the actin cap might have been destroyed and also a direct relation between nuclei morphology and cell stiffness.

5.3.2 Patterned surface validation

In order to validate the best patterned surface, of the two selected (see section 3.2), for the project, it was chosen two parameters, Eccentricity and Extent, to describe the response of the nucleus to each surface.

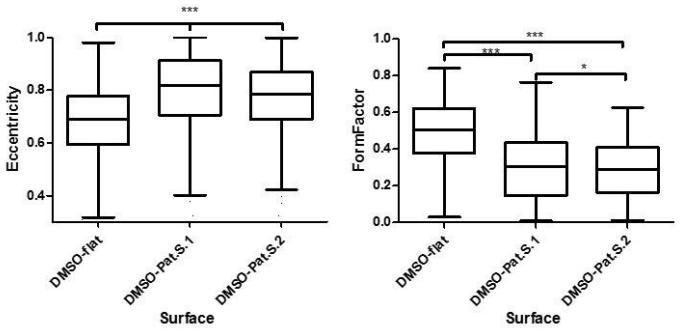

Figure 12 - Representation of Eccentricity and Extent for nuclei in control condition (DMSO) on the three surfaces (Flat, Patterned surface 1 and Patterned surface 2). Statistical analysis by One-way ANOVA (Kruskal Wallis test) showed significance at p-value<0,05.

It was possible to see, based in Figure 12, that patterned surfaces induced the elongation of nuclei (higher eccentricity and lower FormFactor). However, the criteria to select patterned surfaces, explained in section 3.2, was to choose surfaces that affect less possible the nuclei, and by Eccentricity graphs, it could be said that patterned surface 1 deformed more the nuclei compared with patterned surface 2. So, it would be supposed to choose patterned surface 2. Although, the chosen patterned surface was number 1. From principal component analysis (PCA) plot, in Figure 13, it was possible to see that the responses to patterned surface 1, represented by red color, were closer to the flat surface, in black color. While responses to patterned surface 2 were a bit further to flat surface which indicated that response to patterned surface 1 was more similar to unpatterned surface in control condition. Hence both patterned surfaces had long tail, which could indicate that cells had very unique response in comparison to flat surface.

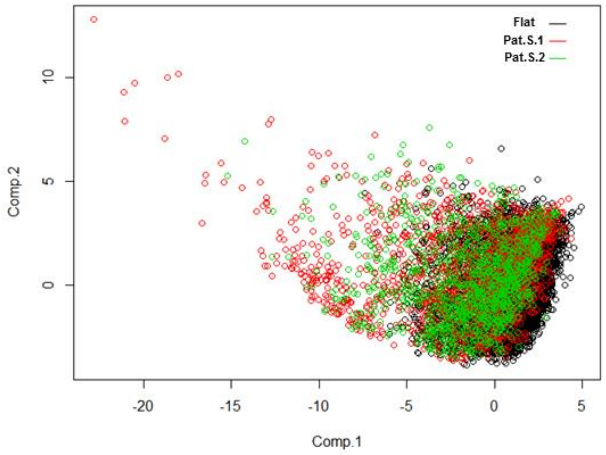

Figure 13 - PCA plot of nuclei morphological data for each surface.

5.3.3 3D Images

Three-dimension images were taken on confocal microscope, of hMSCs on the pattered surface selected. These images allowed to have a general idea of how cells adopt the patterns. The next figure shows three images of cell morphology in different perspectives.

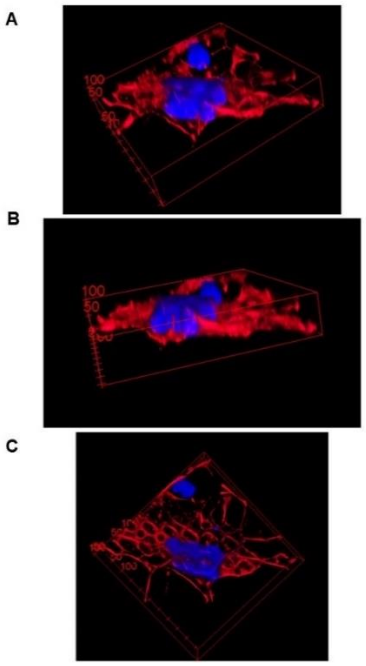

Figure 14 - 3D images of hMSCs on patterned surface 1, in different perspectives. Red color represent Phalloidin and blue color DAPI, actin and nucleus of the cell, respectively. A-Viewed from top; B-Viewed from the side; C-Viewed from the bottom.

From images of Figure 14, it was clearly seen that the actin of cell adopted very well the patterns. The nuclei also tended to adopt the patterns, but the deformation was not so evident compared to actin.

5.4 Using a patterned surface to distinguish cell types

After the validation of the best patterned surface, it was performed an experiment with different cell types, that were seeded in the selected surface, in order to see differences of nuclei morphology of different cell types.

First, it was done a recursive partitioning analysis (Figure 15) to select the most important parameters to distinguish all cell types. The nuclei selected parameters were: Area, Extent, FormFactor, MinorAxisLength, Perimeter and Solidity.

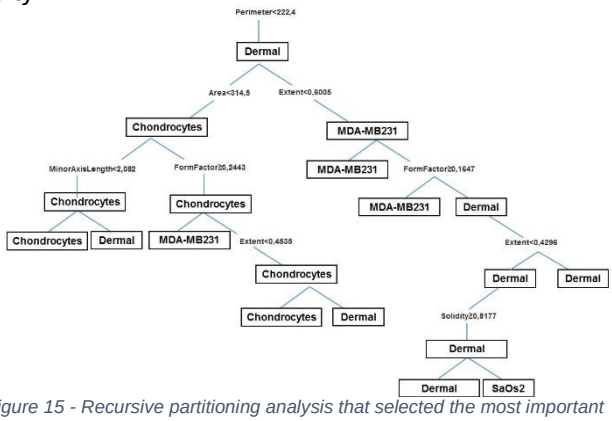

Figure 15 - Recursive partitioning analysis that selected the most important parameters to distinguish all cell types on patterned surface 1.

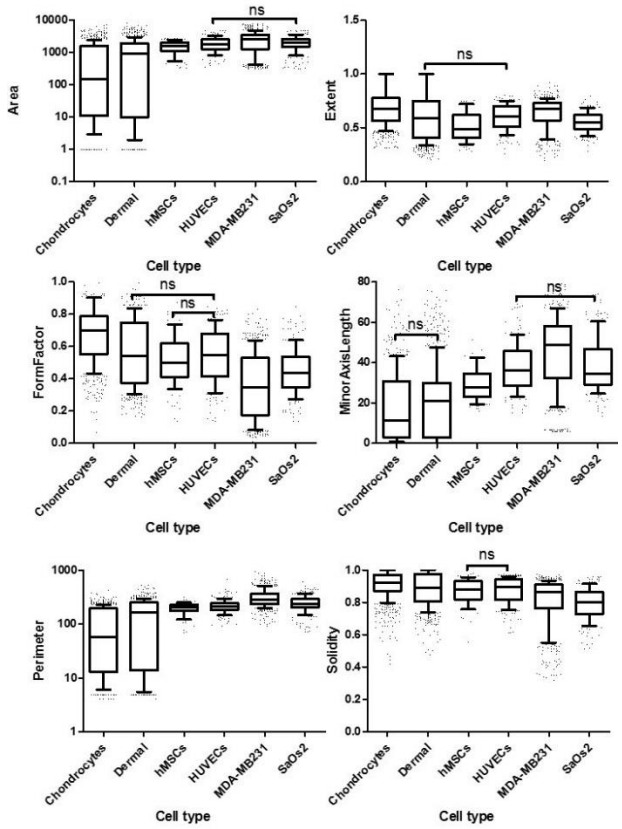

Figure 16 - Graphical representation of nuclei selected parameters for each cell type. Statistical analysis by One-way ANOVA (Kruskal Wallis test) showed significance at p-value<0,05. Non-significant (ns) differences are represented. The remaining differences are statistically significant.

About the Area graph of Figure 16, MDA-MB231 cells were the ones that presented higher values. This could be an evidence of bigger nuclear size for these cells, when compared to the others in study. By the observation of nuclear representative images of each cell type, in Figure 17, in fact the Area of MDA-MB231 cells is higher. For chondrocytes and dermal fibroblast, the area covers a big range of values, which could mean that Cell Profiler did not identify correctly all the objects (nuclei).

Regarding the Extent graph, hMSCs and SaOs2 tended to present lower values of Extent, meaning that they presented some extensions when cultured on this patterned surface. Complementing with Figure 17, SaOs2 nuclei looked to be very deformable, since it seemed to adopt pattern shape.

About FormFactor graph, MDA-MB231 cells are the ones that presented the lowest values, meaning that their nuclei tended to be more rounded, as it can be observed by the respective representative image, in Figure 17. SaOs2 and hMSCs also presented lower FormFactor values, and observing Figure 17, the less elongation of the nuclei can be detected. Chondrocytes, dermal and HUVECs shown the highest values of FormFactor, revealing their nuclei more elongated, as shown by representative images in Figure 17.

Related to MinorAxisLength and Perimeter graphs, the results followed the same trend of Area results, which was in agreement with their definition.

For Solidity, all the values were near 1, which revealed that all cell types had their nuclei in a shape more elongated, according to Solidity definition.

Through these results, each cell type revealed to has a unique response to patterned surfaces. The recursive partitioning tree, in Figure 15, showed that different parameters can revealed different cell types.

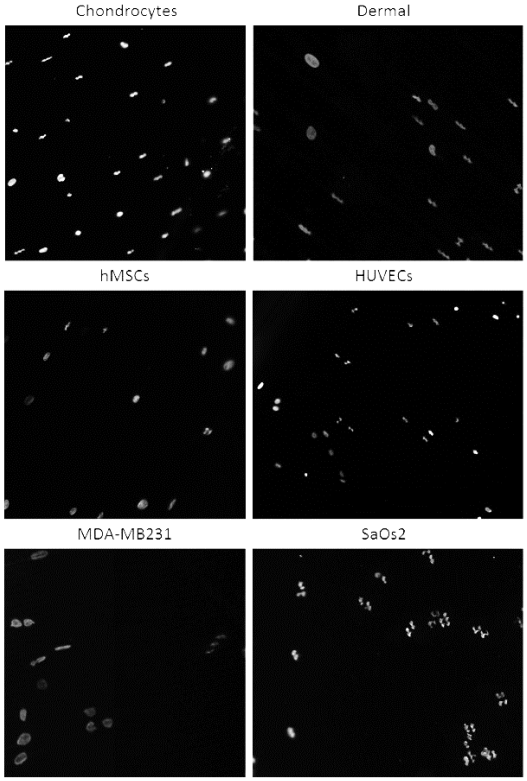

Figure 17 - Representative images of different cell types nuclei on patterned surface.

5.5 Cell stiffness assessment of different cell types based on lamin-A:lamin-B ratio

As said in section 2, nuclear lamins contribute to nuclear stiffness and nuclear stability. Wherein lamin A/C dominates stiff nucleus and lamin B dominates soft nucleus. With that, the stoichiometric ratio of lamins A and B has been used as an indicator of nuclear stiffness. Based on this, the six cell types used in this experiment were ranked according to [8], [17] As mentioned in this literature hMSCs and hCHs tended to assume higher ratios when compared to cancerous cells, like MDA-MB231 and SaOs-2 (hMSCs<hCHs<MDA-MB231 and SaOs-2). It was not found any relevant studies that allowed to conclude about relative stiffness of HUVECs and hDFs.

To complement this assumption, one analysis was performed and the ratios determined for each type of cell in two distinct surfaces: flat and patterned surface 1. The amount of lamins in nuclei was determined based on the respective immunofluorescence detected by Cell Profiler.

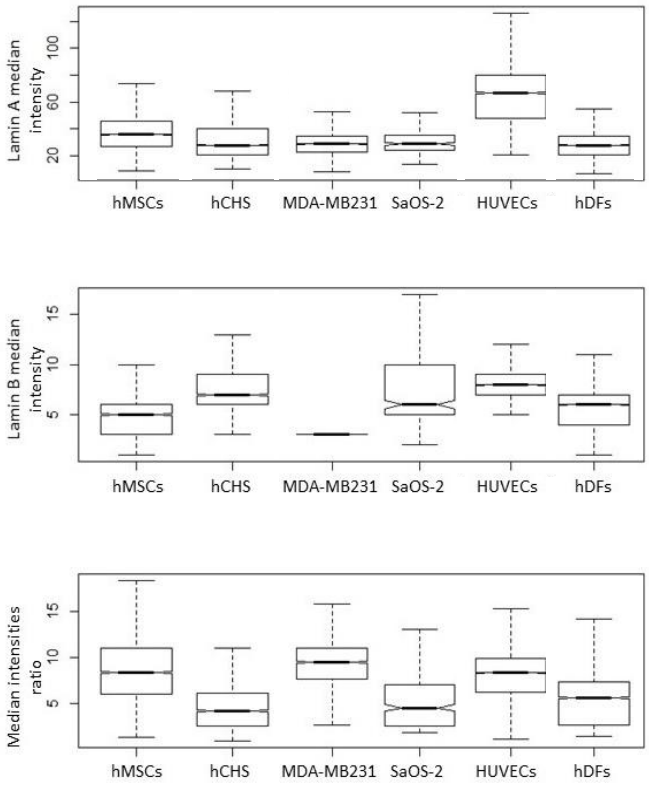

Figure 18 - Schematic representation of lamin A and lamin B normalized median intensities and median intensities ratio for flat surface.

By observing Figure 18, it was possible to see that hMSCs are the cells that presented a higher ratio of lamins, according to literature [17]. This results from a lower lamin B and a higher lamin A. HUVECs presented also a higher ratio, due to the higher amount of lamin A in the nuclei. HCHs presented a lower ratio, high lamin B and low lamin A, compared with hMSCs, which was in accordance with literature [17]. SaOs-2 ratio was among the lowest ratios, since these cells had a considerable amount of lamin B, indicating that the nuclei of this cell type were less stiff. MDA-MB231 ratio was expected to present the same behavior of SaOs-2 ratio, since they are also cancerous cells. However it did not happen, because the analysis of lamin B did not seem to work. In this way, the staining protocol should be optimized for this cells.

From these results, it is possible to show that the stiffness measurements are in agreement with literature [17], except for MDA-MB231 cells. Nuclear stiffness of HUVEC cell lines is somewhere between hMSCs and SaOs2, while for hDFs the nuclear stiffness is close to hCHs. By the observation of SaOs2 and hMSCs representative images in Figure 17, the responses of these cell types were completely different, as also supported by the differences in Solidity parameter, represented in Figure 16. So, it is possible to link the ability of nuclei to deform and their stiffness.

6 Conclusions and Future Perspectives

Object identification by Cell Profiler software is an important step in this project, being the cell density a crucial parameter for this identification efficient. For that, 5000 cells/cm^2 was the cell density selected.

The modulation of cell stiffness was successfully achieved by using Blebb. The treatment showed to be more relevant at 50 µM and during 24h, which revealed a great loss of cytoplasmic coherence and consequently a decrease of stiffness. Through the joint effect of Blebb and TSA treatment, the actin cap might have been destroyed, meaning that, possibly, a direct relation of nuclear morphology and cell stiffness was found. In order to assess cell stiffness, nuclear morphological descriptors were shown to be more robust and less variable in Blebb treatment than cellular morphological descriptors. For that reason, the assessment of cell stiffness was made based on the morphology of nuclei.

The patterned surface that showed to be the most appropriated for studies in this project was the number 1. This one revealed to be more consistent and reportable than number 2, since results, for same treatments, in a flat surface (control situation) and in Pat.S.1 followed the same trend, contrary to the Pat.S.2. Then, the different cell types used in this study could be distinguished by comparing their nuclear morphologic parameters in the patterned surface selected. The parameters considered were: Area, Extent, FormFactor, MinorAxisLength, Perimeter and Solidity. Although, further study should be done to find the most optimal parameters.

For assessing nuclear stiffness, measurements of lamins ratio for each cell type were determined. It was observed that hMSCs presented the highest values, therefore this cells were the ones that presented a higher nuclear stiffness. In the opposite, the cancerous cell type, SaOs2, showed a lower nuclear stiffness. With this, a relation between the ability of nuclei to deform and their stiffness were shown, which means that there is possibility to measure stiffness by cell response.

For future directions, it would be interesting to manipulate the malignancy of cancerous cells and then, try to correlate with their stiffness and their cell response on patterns. Cluster different cell types based on their shape and stiffness would be also valuable. Further research should

be directed to investigate a single parameter that can assess general cell deformation.

7 References

[1] K. a Kilian, B. Bugarija, B. T. Lahn, and M. Mrksich, “Geometric cues for directing the differentiation of mesenchymal stem cells.,” *Proc. Natl. Acad. Sci. U. S. A.*, vol. 107, no. 11, pp. 4872–7, Mar. 2010.

[2] R. McBeath, D. M. Pirone, C. M. Nelson, K. Bhadriraju, and C. S. Chen, “Cell shape, cytoskeletal tension, and RhoA regulate stem cell lineage commitment.,” *Dev. Cell*, vol. 6, no. 4, pp. 483–95, Apr. 2004.

[3] E. Paluch and C.-P. Heisenberg, “Biology and physics of cell shape changes in development.,” *Curr. Biol.*, vol. 19, no. 17, pp. R790–9, Sep. 2009.

[4] P. Isermann and J. Lammerding, “Nuclear mechanics and mechanotransduction in health and disease.,” *Curr. Biol.*, vol. 23, no. 24, pp. R1113–21, Dec. 2013.

[5] Y. Ren, J. C. Effler, M. Norstrom, T. Luo, R. A. Firtel, P. A. Iglesias, R. S. Rock, and D. N. Robinson, “Mechanosensing through cooperative interactions between myosin II and the actin crosslinker cortexillin I.,” *Curr. Biol.*, vol. 19, no. 17, pp. 1421–8, Sep. 2009.

[6] K. N. Dahl, A. J. S. Ribeiro, and J. Lammerding, “Nuclear shape, mechanics, and mechanotransduction.,” *Circ. Res.*, vol. 102, no. 11, pp. 1307–18, Jun. 2008.

[7] P. Matheiu and E. Loboa, “Cytoskeletal and Focal Adhesion Influences on Mesenchymal Stem Cell Shape, Mechanical Properties, and differentiation down osteogentic, adipogenic, and chondtogenic pathways,” *Tissue Eng. Part B. Rev.*, vol. 18, no. 6, pp. 436–444, Dec. 2012.

[8] P. M. Davidson, H. Özçelik, V. Hasirci, G. Reiter, and K. Anselme, “Microstructured surfaces cause severe but non-detrimental deformation of the cell nucleus,” *Adv. Mater.*, vol. 21, no. 35, pp. 3586–3590, Sep. 2009.

[9] P. M. Davidson, O. Fromigué, P. J. Marie, V. Hasirci, G. Reiter, and K. Anselme, “Topographically induced self-deformation of the nuclei of cells: dependence on cell type and proposed mechanisms.,” *J. Mater. Sci. Mater. Med.*, vol. 21, no. 3, pp. 939–46, Mar. 2010.

[10] M. Vicente-Manzanares, X. Ma, R. S. Adelstein, and A. R. Horwitz, “Non-muscle myosin II takes centre stage in cell adhesion and migration.,” *Nat. Rev. Mol. Cell Biol.*, vol. 10, no. 11, pp. 778–90, Nov. 2009.

[11] N. Wang, J. D. Tytell, and D. E. Ingber, “Mechanotransduction at a distance: mechanically coupling the extracellular matrix with the nucleus.,” *Nat. Rev. Mol. Cell Biol.*, vol. 10, no. 1, pp. 75–82, Jan. 2009.

[12] M. Versaevel, T. Grevesse, and S. Gabriele, “Spatial coordination between cell and nuclear shape within micropatterned endothelial cells.,” *Nat. Commun.*, vol. 3, p. 671, Jan. 2012.

[13] S. B. Khatau, D.-H. Kim, C. M. Hale, R. J. Bloom, and D. Wirtz, “The perinuclear actin cap in health and disease.,” *Nucleus*, vol. 1, no. 4, pp. 337–42, 2010.

[14] S. B. Khatau, C. M. Hale, P. J. Stewart-Hutchinson, M. S. Patel, C. L. Stewart, P. C. Searson, D. Hodzic, and D. Wirtz, “A perinuclear actin cap regulates nuclear shape.,” *Proc. Natl. Acad. Sci. U. S. A.*, vol. 106, no. 45, pp. 19017–22, Nov. 2009.

[15] M. Versaevel, M. Riaz, T. Grevesse, and S. Gabriele, “Cell confinement: putting the squeeze on the nucleus,” *Soft Matter*, vol. 9, no. 29, p. 6665, 2013.

[16] P. Jevtić, L. J. Edens, L. D. Vuković, and D. L. Levy, “Sizing and shaping the nucleus: mechanisms and significance.,” *Curr. Opin. Cell Biol.*, vol. 28, pp. 16–27, Jun. 2014.

[17] J. Swift, I. L. Ivanovska, A. Buxboim, T. Harada, P. C. D. P. Dingal, J. Pinter, J. D. Pajerowski, K. R. Spinler, J.-W. Shin, M. Tewari, F. Rehfeldt, D. W. Speicher, and D. E. Discher, “Nuclear lamin-A scales with tissue stiffness and enhances matrix-directed differentiation.,” *Science*, vol. 341, no. 6149, p. 1240104, Aug. 2013.

[18] J. Lammerding, P. C. Schulze, T. Takahashi, S. Kozlov, T. Sullivan, R. D. Kamm, C. L. Stewart, and R. T. Lee, “Lamin A/C deficiency causes defective nuclear mechanics and mechanotransduction.,” *J. Clin. Invest.*, vol. 113, no. 3, pp. 370–8, Feb. 2004.

[19] A. Mazumder, T. Roopa, A. Basu, L. Mahadevan, and G. V Shivashankar, “Dynamics of chromatin decondensation reveals the structural integrity of a mechanically prestressed nucleus.,” *Biophys. J.*, vol. 95, no. 6, pp. 3028–35, Sep. 2008.

[20] J. Rao, D. Bhattacharya, B. Banerjee, A. Sarin, and G. V. Shivashankar, “Trichostatin-A induces differential changes in histone protein dynamics and expression in HeLa cells,” *Biochem. Biophys. Res. Commun.*, vol. 363, no. 2, pp. 263–268, Nov. 2007.

[21] G. Wang, W. Mao, R. Byler, K. Patel, C. Henegar, A. Alexeev, and T. Sulchek, “Stiffness dependent separation of cells in a microfluidic device.,” *PLoS One*, vol. 8, no. 10, p. e75901, Jan. 2013.

[22] J. Guck, S. Schinkinger, B. Lincoln, F. Wottawah, S. Ebert, M. Romeyke, D. Lenz, H. M. Erickson, R. Ananthakrishnan, D. Mitchell, J. Käs, S. Ulvick, and C. Bilby, “Optical deformability as an inherent cell marker for testing malignant transformation and metastatic competence.,” *Biophys. J.*, vol. 88, no. 5, pp. 3689–98, May 2005.

[23] M. Krause, J. Te Riet, and K. Wolf, “Probing the compressibility of tumor cell nuclei by combined atomic force-confocal microscopy.,” *Phys. Biol.*, vol. 10, no. 6, p. 065002, Dec. 2013.

[24] J. Eyckmans, T. Boudou, X. Yu, and C. S. Chen, “A hitchhiker’s guide to mechanobiology.,” *Dev. Cell*, vol. 21, no. 1, pp. 35–47, Jul. 2011.

[25] M. L. Gardel, K. E. Kasza, C. P. Brangwynne, J. Liu, and D. a Weitz, “Chapter 19: Mechanical response of cytoskeletal networks.,” *Methods Cell Biol.*, vol. 89, no. 08, pp. 487–519, Jan. 2008.

[26] M. J. Poellmann, P. A. Harrell, W. P. King, and A. J. Wagoner Johnson, “Geometric microenvironment directs cell morphology on topographically patterned hydrogel substrates.,” *Acta Biomater.*, vol. 6, no. 9, pp. 3514–23, Oct. 2010.

[27] Z. Pan, C. Yan, R. Peng, Y. Zhao, Y. He, and J. Ding, “Control of cell nucleus shapes via micropillar patterns.,” *Biomaterials*, vol. 33, no. 6, pp. 1730–5, Mar. 2012.

[28] H. V Unadkat, M. Hulsman, K. Cornelissen, B. J. Papenburg, R. K. Truckenmüller, A. E. Carpenter, M. Wessling, G. F. Post, M. Uetz, M. J. T. Reinders, D. Stamatialis, C. a van Blitterswijk, and J. de Boer, “An algorithm-based topographical biomaterials library to instruct cell fate.,” *Proc. Natl. Acad. Sci. U. S. A.*, vol. 108, no. 40, pp. 16565–70, Oct. 2011.

[29] J. C. Meredith, “Advances in combinatorial and high-throughput screening of biofunctional polymers for gene delivery, tissue engineering and anti-fouling coatings,” *J. Mater. Chem.*, vol. 19, no. 1, p. 34, Dec. 2009.

[30] A. E. Carpenter, T. R. Jones, M. R. Lamprecht, C. Clarke, I. H. Kang, O. Friman, D. a Guertin, J. H. Chang, R. a Lindquist, J. Moffat, P. Golland, and D. M. Sabatini, “CellProfiler: image analysis software for identifying and quantifying cell phenotypes.,” *Genome Biol.*, vol. 7, no. 10, p. R100, Jan. 2006.

[31] E. K. F. Yim, S. W. Pang, and K. W. Leong, “Synthetic nanostructures inducing differentiation of human mesenchymal stem cells into neuronal lineage.,” *Exp. Cell Res.*, vol. 313, no. 9, pp. 1820–9, May 2007.

[32] Z. Liu, L. a van Grunsven, E. Van Rossen, B. Schroyen, J.-P. Timmermans, A. Geerts, and H. Reynaert, “Blebbistatin inhibits contraction and accelerates migration in mouse hepatic stellate cells.,” *Br. J. Pharmacol.*, vol. 159, no. 2, pp. 304–15, Jan. 2010.